Supported rhenium nanoparticle catalysts for acceptorless dehydrogenation of alcohols: structure-activity relationship and mechanistic studies

Kenichi Kon [a], Wataru Onodera[a], Takashi Toyao,[a,b,]* Ken-ichi Shimizu [a,b,]*

[a] Institute for Catalysis, Hokkaido University, N-21, W-10, Sapporo 001-0021, Japan

[b] Elements Strategy Initiative for Catalysts and Batteries, Kyoto University, Katsura, Kyoto 615-8520, Japan

***Corresponding author**

Ken-ichi Shimizu

Institute for Catalysis, Hokkaido University, N-21, W-10, Sapporo 001-0021, Japan, E-mail: kshimizu@cat.hokudai.ac.jp, Fax: +81-11-706-9163, Tel: +81-11-706-9164

Abstract

Al_2O_3-supported Re with different oxidation state and Re^0 metal nanoparticles on various supports are prepared, characterized, and tested for the dehydrogenation of 2-octanol. The activity of Re/Al_2O_3 increases with the fraction of metallic Re. The activity of metallic Re depends on the support oxides, and the support with moderate electronegativity (Al_2O_3) gives the highest turnover frequency (TOF) per surface Re^0 sites. Re/Al_2O_3 is effective for acceptorless dehydrogenation of various aliphatic secondary alcohols to ketones. The kinetic isotope effects on the dehydrogenation of 2-propanol show that dissociation of α-C-H bond of 2-propanol is the rate limiting step. IR study of the reaction of gas phase 2-propanol over Re/Al_2O_3 surface shows that the acid-base pair site of Al_2O_3 is responsible for the O-H dissociation of 2-propanol. The structural requirements are discussed on the basis of the mechanistic results.

Keywords: alcohols · dehydrogenation· nanoparticles · rhenium

Introduction

Catalytic acceptorless dehydrogenation of alcohols to carbonyl compounds and H_2 has been an attractive area of research in catalysis, sustainable energy and organic synthesis.[1,2] Previous attempts have been mainly focused on Ru- or Ir -based homogeneous catalysts.[1-7] However, most of the homogeneous catalysts suffer from drawbacks such as needs of an acid or base additive and expensive ligands and difficulties in separation and recycle of the catalyst. To meet environmental and economical acceptability, efforts have been devoted to heterogeneous

catalytic systems for acceptorless dehydrogenation of alcohols.[8-20] However, rational improvement of the catalytic efficiency of heterogeneous catalyst for this reaction is still difficult due to a lack of fundamental information on the structure–activity relationship and reaction mechanism. For example, controversial models are proposed on the oxidation states of transition metal catalysts for this reaction; metallic species are proposed to be effective for the supported Ag,[17] Co,[18] Ni[19] and Pt[20] catalysts, whereas Re^0-core/ReO_2-shell model is proposed as an active Re species of unsupported nanocrystalline catalyst.[16]

As our continuous studies on the structural and mechanistic aspects of supported transition metal catalysts for this reaction,[17-20] we report herein the effects of oxidation state of Re and support materials on heterogeneous Re catalysis for the dehydrogenation of secondary alcohols. It will be shown that metallic Re sites and acid-base pair sites on the support are key elements in this catalytic system. Spectroscopic and kinetic studies will suggest mechanistic roles of the metallic Re site and the acid-base sites.

Results and Discussion

Effect of Re Oxidation State on the Activity of Re/Al_2O_3

To study the dependence of the catalytic activity on the mean oxidation state of Re/Al_2O_3, first we prepared Re/Al_2O_3 catalysts with different oxidation state by changing the H_2-reduction temperature of the oxidic precursor, $ReOx/Al_2O_3$. Figure 1A shows Fourier transforms of X-ray absorption fine structure (EXAFS) of $ReOx/Al_2O_3$ and the catalysts reduced at 200, 300, 400, and 500 ˚C. The results of curve fitting analysis of the EXAFS are listed in Table 1, and the coordination numbers of Re-O and Re-Re shells are plotted as a function of the H_2-reduction temperature in Figure 2. The EXAFS of $ReOx/Al_2O_3$ consists of a Re-O shell at bond distance (R) of 1.74 Å with coordination number (N) of 4.8, and these values are close to the reported data of NH_4ReO_4 (R = 1.74 Å, N = 4).[21a,22] This indicates that the Re species in $ReOx/Al_2O_3$ have perrhenate-like structure with the oxidation state of Re^{7+}. A recent EXAFS study of $ReOx/SiO_2$ also reported similar EXAFS results and proposed the same structural model.[21a] The EXAFS of the sample after reduction at 200 ˚C also consists of the Re-O shell (1.74 Å) with lower coordination number (N = 2.4). This suggests that Re species in the sample are Re oxides with lower number of Re-O bonds, or in other words Re oxides with the lower valence than those in $ReOx/Al_2O_3$ (Re^{7+}). Figure 1B shows Re L_3-edge X-ray absorption near-edge structures (XANES). It is established that decrease in the average valence of Re species results in decrease in the intensity of the $2p_{3/2}\rightarrow 5d$ peak named white line, and hence the area intensity of the white line is an index of the oxidation state of Re species.[21] The XANES spectrum of the sample reduced at 200 ˚C (spectrum b) shows smaller intensity of the $2p_{3/2}\rightarrow 5d$ peak (10537 eV) than $ReOx/Al_2O_3$ (spectrum a). This shows that reduction of $ReOx/Al_2O_3$ at 200 ˚C

decreases the average valence of Re, which is consistent with the EXAFS result. The EXAFS of the samples after the reduction treatments at 300 and 400 ˚C consist of two shells (Re-O shell at 2.01-2.10 Å and Re-Re shell at 2.74 Å). The EXAFS of the samples after reduction at 500 ˚C consists of a Re-Re shell at 2.74 Å, indicating that the sample consists of only metallic Re species.[21] As plotted in Figure 2, the Re-O coordination number decreases with increasing H_2-reduction temperature, while the Re-Re coordination number increases with the reduction temperature. These results indicate that the perrhenate (Re^{7+})-like species in $ReOx/Al_2O_3$ are gradually reduced to give the metallic Re by the reduction at higher temperature. This is consistent with the XANES result that the intensity of the $2p_{3/2}\rightarrow 5d$ peak decreases with the reduction temperature (Figure 1B).

To quantify the average valence of Re species in the samples, we estimated the area of the $2p_{3/2}\rightarrow 5d$ peak in the Re L_3-edge XANES spectra by the method adopted in our previous studies of Pd and Rh L_3-edge XANES analyses.[23,24] As illustrated in Figure 3, an arctangent function shown as a dashed line, corresponding to the continuum absorption, was subtracted from the raw spectrum (dots) to give the absorption due to the electron transition from $2p_{3/2}$ to $5d_{3/2}$ and $5d_{5/2}$ (solid line). The white line area intensities estimated are plotted in Figure 2 as a function of the reduction temperature. The result quantitatively indicates that the white line area, or in other words, the average valence of Re decreases with the reduction temperature. This tendency is consistent with the tendency in the coordination numbers from EXAFS analysis co-plotted in Figure 2; the metallic Re species became dominant at higher the reduction temperature.

As evidenced by the structural results, we have prepared a series of Re-loaded Al_2O_3 catalysts with different average oxidation states. Using the catalysts reduced at 200, 300, 400, and 500 ˚C, next we carried out a model dehydrogenation of 2-octanol to 2-octanone under the same reaction conditions (under N_2 in reflux conditions in *o*-xylene for 0.5 h). The initial rates per total number of Re atom in the catalyst were determined under the conversion levels below 20% and were plotted as a function of the reduction temperature in Figure 2. The reaction rate increases with the reduction temperature, and this tendency coincides with the decrease in the valence of Re species (increase in the fraction of metallic Re species) with the reduction temperature. The result clearly indicates that the metallic Re species are catalytically important species in the acceptorless dehydrogenation of the alcohol by the heterogeneous Re catalysts. This conclusion is consistent with our previous conclusions on the valence state of the transition metals (Ag,[17] Co,[18] Ni,[19] Pt[20])-loaded catalysts for the dehydrogenation of the alcohol. Hence, it can be generally concluded that metallic species are the active species in the acceptorless dehydrogenation of alcohols by the supported transition metal catalysts.

Structure and Performance of the Standard Re/Al_2O_3 Catalyst

The above chapter shows that the Re/Al_2O_3 catalyst reduced at 500 ˚C, consisting of only metallic Re species, is the most active catalyst in the Al_2O_3-supported Re catalysts tested. Based on various characterization results, here we discuss the structure of this standard catalyst hereafter designated as Re/Al_2O_3. The EXAFS result (Table 1) of this sample shows smaller Re-Re coordination number (8.9) than that of bulk Re metal (12),[21] which is characteristic to metal nanoparticles with a small mean diameter. To estimate the particle size, we carried out TEM analysis of Re/Al_2O_3. As shown in the representative picture (Figure 4), a few nm sized semi-spherical Re metal nanoparticles were observed. The analysis of the particle size distributions (Figure 4) showed the mean particle diameter of 4.2 ± 1.1 nm, corresponding to the volume-area mean diameter[25] of 5.2 ± 1.1 nm. The volume-area mean diameters (5.2 ± 1.1 nm) estimated by TEM analysis is consistent with those estimated by the CO adsorption experiment (4.6 nm) within the experimental error of the TEM analysis, which indicates that the mean Re size from the CO adsorption is the accurate.

Table 2 shows the catalytic performance of the standard Re/Al_2O_3 catalyst for dehydrogenation of various alcohols. In the presence of 1 mol% of Re/Al_2O_3 powder, containing 0.01 mmol of Re, 1 mmol of various aliphatic secondary alcohols were selectively converted to the corresponding ketones with good yields (72-96%). For the reaction of cyclooctanol (entry 1), turnover number (TON) with respect to the total Re atoms in the catalysts is 84, which is higher than the TON (50) of the recently reported unsupported Re nanoparticle catalyst at higher reaction temperature (180 ˚C).[16]

Effect of Supports on the Activity of Re Catalysts

Next, we prepared a series of 5 wt% Re-loaded catalysts with different support materials. The mean particle size of the Re metal particles on each catalyst was estimated by the CO adsorption. Table 3 lists the reduction temperature, mean size of Re metal particles, of the catalysts together with the averaged electronegativity of metal oxide supports. Note that the catalyst was reduced under H_2 at different temperatures (T_{H2}) in order to prepare the catalysts with the similar Re particle size (3.9-6.6 nm) but with different support materials.

With the catalysts in Table 3, we studied influence of supports on the catalytic activity for dehydrogenation of 2-octanol to 2-octanone under the same reaction conditions (under N_2 in reflux conditions for 0.5 h). Using the number of Re^0 sites estimated by the CO adsorption experiment, the initial rates were converted to the turnover frequency (TOF) per surface Re^0 sites (Table 4). The activity (TOF) depended strongly on the support material, and Re/Al_2O_3 was found to give the highest activity. Al_2O_3 itself was inactive (result not shown). To discuss the support effect, Figure 5 plots TOF versus the electronegativity of the support metal oxide, which

is generally used as a parameter of acidity of metal oxides.[26] There is a volcano-type relationship between TOF and the electronegativity of the support. Basic supports (MgO, La_2O_3, La_2O_3) and acidic supports (Nb_2O_5, SnO_2) show lower activity than amphoteric oxide supports (CeO_2, Al_2O_3, TiO_2). Taking into account the result in Table 4 that Re nanoparticles supported on nearly neutral supports (SiO_2 and carbon) gave an order of magnitude lower TOF than those on the amphoteric oxide supports (CeO_2, Al_2O_3, TiO_2), it is shown that the strong support effect in this catalytic system is caused by the acid-base characteristics of the supports and amphoteric (acid-base bifunctional) nature gives positive effect on the activity of the supported Re.

Reaction Mechanism

To investigate reaction mechanism, in situ IR experiments on the reaction of gas phase 2-propanol with the surface of Re/Al_2O_3 was carried out at 80 ˚C. Figure 6A shows the spectra of adsorbed species formed by the pulse injection of 2-propanol-O-d, $(CH_3)_2CHOD$, over Re/Al_2O_3 which was in situ pre-reduced at 500 ˚C. Initially (t = 120 s), the bands due to 2-propoxide (2973, 1467, 1164, 1130 cm^{-1}) and Al-OD (2530 cm^{-1}) on the Al_2O_3 surface, were observed in the IR spectrum. We have previously reported the same IR experiment for pure Al_2O_3.[20] The positions of the bands for Re/Al_2O_3 are essentially the same as those for Al_2O_3.[20] This indicates that 2-propoxide and D^+ ions are adsorbed not on Re but on the Al_2O_3 surface (Eqn. 1).

$$2Al\text{-}O + (CH_3)_2CHOD \rightarrow (CH_3)_2CH\text{-}O\text{-}Al + Al\text{-}OD \qquad (1)$$

Figure 6B shows the height of the bands due to 2-propoxide (Al-O*i*Pr), Al-OD and adsorbed acetone as a function of time in a flow of He. With increase in the reaction time, intensity of the bands due to the 2-propoxide species decreased and a band at 1698 cm^{-1} due to C=O stretching of adsorbed acetone appeared. The same IR experiment with pure Al_2O_3 gave no bands due to acetone under the same conditions (results not shown). These results suggest that Re metal is responsible for C-H dissociation of the 2-propoxide to yield acetone (Eqn. 2). Figure 6 shows that the formation of 2-propoxide finished within 120 s, while its decrease took more than 1000 s. This indicates that the formation of 2-propoxide is faster than the dehydrogenation of 2-propoxide to acetone. Therefore, the O-D dissociation of $(CH_3)_2CHOD$ is faster than α-C-H dissociations of the 2-propoxide.

$$(CH_3)_2CH\text{-}O\text{-}Al + Re^0 \rightarrow (CH_3)_2C{=}O + Al\text{-}O + Re\text{-}H \qquad (2)$$

The intensity of the band due to Al-OD (2530 cm^{-1}) decreased with time. This can be explained by the reaction of Re-H with AlOD to yield dihydrogen (HD), accompanying the regenerations of the Re^0 and Al-O sites (Eqn. 3).

$$Re\text{-}H + Al\text{-}OD \rightarrow HD + Re^0 + Al\text{-}O \qquad (3)$$

We also studied kinetic isotope effect (KIE) in the liquid phase 2-propanol dehydrogenation by

Re/Al_2O_3 in toluene under refluxing conditions. Figure 7 shows the kinetic curves for the formation of acetone from $(CH_3)_2CHOH$, $(CH_3)_2CHOD$ and $(CH_3)_2CDOH$. Initially, the amount of acetone linearly increased with the reaction time, and hence the initial slope corresponds to the zero order rate constant. Using the rate constants for $(CH_3)_2CHOH$ and $(CH_3)_2CHOD$, the KIE (k_H/k_D) was estimated to be 1.9, which is classified as secondary KIE.[27] The kinetic isotope effect from the data of $(CH_3)_2CHOH$ and $(CH_3)_2CDOH$ showed the primary KIE[27] of 7.6. The results indicate that the α-C-H dissociation of 2-propanol is the rate limiting steps. Taking into account the IR result that the formation of 2-propoxide is faster than its dehydrogenation, the secondary KIE of 1.9 observed for $(CH_3)_2CHOH$ and $(CH_3)_2CHOD$ suggests that a step involving D other than the dissociation of O-D in $(CH_3)_2CHOD$ is relatively slow. Considering the reaction mechanism in Eqn. (1)-(3), the most probable step that can show KIE of 1.9 is the O-D dissociation step in the reaction of Re-H with AlOD (Eqn. 3). Therefore, the KIE of 1.9 observed for $(CH_3)_2CHOH$ and $(CH_3)_2CHOD$ is an indirect evidence of the cooperative function of Al_2O_3 surface during the H_2 formation step (Eqn. 3). The cooperative function of Al_2O_3 involves both deprotonation (Eqn. 1) and protonation (Eqn. 3), possibly caused by the basic and acidic functions of Al_2O_3. This is a possible reason why the Re-catalyzed dehydrogenation of alcohols requires acid-base bifunctional supports (Figure 5). It is important to note that the cooperative mechanism in Eqn. (1)-(3) is similar to those proposed in our previous studies on Ag-,[17] Co-,[18] Ni-,[19] and Pt[20]-loaded Al_2O_3 catalysts.

4. Conclusion

The Al_2O_3-supported Re nanoparticle were found to be efficient heterogeneous catalyst for the acceptorless dehydrogenation of secondary alcohols. Re metal particles supported on amphoteric supports (CeO_2, Al_2O_3, TiO_2) showed higher TOF per surface Re sites than those on acidic and basic supports. IR results show that fast dissociation of alcohol to alkoxide and proton occurs on the Al_2O_3 surface, while Re metal is responsible for C-H dissociation of the alkoxide. The primary KIE of 7.9 for the dehydrogenation of $(CH_3)_2CHOH$ and $(CH_3)_2CDOH$ showed that dissociation of α-C-H bond of 2-propanol was the rate limiting step. Combined with the IR results, the secondary KIE of 1.9 for $(CH_3)_2CHOH$ and $(CH_3)_2CHOD$ suggests the reaction of Re-H with AlOD as a H_2 formation step. The cooperative functions of Al_2O_3 (deprotonation and protonation) are the reason why the Re-catalyzed dehydrogenation of alcohols requires acid-base bifunctional supports.

Acknowledgment

This work was supported by Grant-in-Aids for Scientific Research B (26289299) from MEXT (Japan), a MEXT program “Elements Strategy Initiative to Form Core Research Center” and a

Grant-in-Aid for Scientific Research on Innovative Areas “Nano Informatics” (25106010) from JSPS.

Experimental

General

Commercially available organic compounds (Tokyo Chemical Industry) were used without further purification. 2-Propanol-O-d, $(CH_3)_2CHOD$ with 98 atom % D, and 2-propanol-2-d1, $(CH_3)_2CDOH$ with 99.4 atom % D, were purchased from Sigma-Aldrich. The GC (Shimadzu GC-14B) and GCMS (Shimadzu GCMS-QP2010) analyses were carried out with Ultra ALLOY capillary column UA$^+$-1 (Frontier Laboratories Ltd.) or CP-PoraBOND Q capillary column (Varian) using nitrogen or He as the carrier gas.

Catalyst preparation

Al_2O_3 (mainly θ-phase, surface area of 75m^2 g^{-1}) was prepared by calcination of γ-AlOOH (Catapal B Alumina purchased from Sasol) for 1 h at 1100 °C. SiO_2 (Q-10, 300 m^2 g^{-1}) was supplied from Fuji Silysia Chemical Ltd. TiO_2 (JRC-TIO4, 50 m^2 g^{-1}), MgO (JRC-MGO-3, 19 m^2 g^{-1}) and CeO_2 (JRC-CEO3, 81 m^2 g^{-1}) were supplied from Catalysis Society of Japan. Active carbon (296 m^2 g^{-1}) was purchased from Kishida Chemical. H_2SnO_3 (Kojundo Chemical Laboratory Co., Ltd.) and $Nb_2O_5{\cdot}nH_2O$ (supplied by CBMM) were commercially supplied. Hydroxides of Y and La were prepared by hydrolysis of metal nitrates in distilled water by gradually adding an aqueous NH_4OH solution (1 mol dm^{-3}), followed by filtration of precipitate, washing with distilled water three times, drying at 100 °C for 12 h. Y_2O_3, La_2O_3, Nb_2O_5 and SnO_2 were prepared by calcination of the hydroxides at 500 °C for 3 h.

Re/Al_2O_3 catalysts with Re content of 5 wt% were prepared by an impregnation method. A mixture of Al_2O_3 and an aqueous solution of NH_4ReO_4 was evaporated at 50 °C, followed by drying at 90 °C for 12 h, calcination in air at 300 °C for 1 h, and by in situ pre-reduction in a glass (pyrex or quartz) tube under a flow of H_2 (20 cm^3 min^{-1}) at different reduction temperatures (T_{H2}) for 0.5 h. Other 5 wt% Re-loaded catalysts on different supports were prepared by a similar method.

Characterization

The number of surface metal atoms in the Re catalysts, pre-reduced in H_2 at T_{H2} (in Table 3) was estimated from the CO uptake of the samples at room temperature using the pulse-adsorption of CO in a flow of He by BELCAT (MicrotracBELL Corp.). The CO adsorption experiments for the Re-loaded basic oxides (MgO, Y_2O_3, La_2O_3, CeO_2) were carried out at -78 °C.[28] The average particle size in Table 3 was calculated from the CO uptake assuming that CO was adsorbed on the surface of semispherical Re particles at CO/(surface Re atom) = 1/1 stoichiometry. Transmission electron microscopy (TEM) measurements were

carried out by using a JEOL JEM-2100F TEM operated at 200 kV.

X-ray absorption near-edge structures (XANES) and X-ray absorption fine structure (EXAFS) at Re L_3-edge were measured in transmission mode at the BL-9C of KEK-PF (Tsukuba, Japan) with a ring energy of 2.5 GeV and a stored current of 250–350 mA (Proposal No. 2014P003). The storage ring was operated at 8 GeV. A Si(111) single crystal was used to obtain a monochromatic X-ray beam. The catalysts pre-reduced in a flow of 100% H_2 (20 cm^3 min^{-1}) for 0.5 h at different temperatures (200-500 °C) were cooled to room temperature in the flow of H_2 and were sealed in the cells made of polyethylene under N_2. Then, the EXAFS spectrum of the sealed sample was taken at room temperature. The EXAFS analysis was performed using the REX version 2.5 program (RIGAKU). The parameters for the Re–O and Re–Re shells were provided by the FEFF6.

In situ IR spectra were recorded on a JASCO FT/IR-4200 equipped with a quartz IR cell connected to a conventional flow reaction system. The sample was pressed into a 40 mg self-supporting wafer (ϕ = 2 cm) and mounted into the quartz IR cell with CaF_2 windows. Spectra were measured accumulating 15 scans at a resolution of 4 cm^{-1}. A reference spectrum of the catalyst wafer in He taken at measurement temperature was subtracted from each spectrum. Prior to each experiment the catalyst disk was heated in H_2 flow (100 cm^3 min^{-1}) at 500 °C for 0.5 h, followed by cooling to 80 °C and purging with He.

Condition of catalytic reactions

Re/Al_2O_3 reduced at 500 °C was used as the standard catalyst. After the pre-reduction at 500 °C, we carried out catalytic tests using a batch-type reactor without exposing the catalyst to air as follows. The mixture of *o*-xylene (1 mL), alcohol (1 mmol), and *n*-dodecane (0.2 mmol) was injected to the pre-reduced catalyst inside the reactor (cylindrical glass tube) through a septum inlet, followed by filling N_2. Then, the resulting mixture was stirred under reflux; typically, the bath temperature was 155 °C and reaction temperature was *ca* 144 °C. Conversion and yields of products were determined by GC using *n*-dodecane as an internal standard. Progress of the reaction was monitored by GC analysis of aliquots (ca. 0.02 g). The initial rate of reaction was measured under the conditions where the conversion was below 20%. The products were identified by GC-MS equipped with the same column as GC and by comparison with commercially pure products.

References

1 M. Trincado, D. Banerjee and H. Grützmacher, *Energy Environ. Sci.*, 2014, **7**, 2464–2503.

2 T. C. Johnson, D. J. Morris and M. Wills, *Chem. Soc. Rev.*, 2010, **39**, 81–88.

3 J. Zhang, M. Gandelman, L. J. W. Shimon, H. Rozenberg and D. Milstein, *Organometallics*, 2004, **23**, 4026–4033.

4 K.-i. Fujita, N. Tanino and R. Yamaguchi, *Org. Lett.*, 2007, **9**, 109–111.

5 S. Musa, I. Shaposhnikov, S. Cohen and D. Gelman, *Angew. Chem. Int. Ed.*, 2011, **50**, 3533–3537.

6 R. Kawahara, K.-i. Fujita and R. Yamaguchi, *Angew. Chem. Int. Ed.*, 2012, **51**, 12790–12794.

7 M. Nielsen, E. Alberico, W. Baumann, H.-J. Drexler, H. Junge, S. Gladiali and M. Beller, *Nature*, 2013, **495**, 85–89.

8 M. Yamashita, F. Dai, M. Suzuki and Y. Saito, *Bull. Chem. Soc. Jpn.*, 1991, **64**, 628–634.

9 J. H. Choi, N. Kim, Y. J. Shin, J. H. Park and J. Park, *Tetrahedron Lett.,* 2004, **45**, 4607–4610.

10 W. H. Kim, I. S. Park and J. Park, *Org. Lett.*, 2006, **8**, 2543–2545.

11 T. Mitsudome, Y. Mikami, H. Funai, T. Mizugaki, K. Jitsukawa and K. Kaneda, *Angew. Chem. Int. Ed.*, 2008, **47**, 138–141.

12 T. Mitsudome, Y. Mikami, K. Ebata, T. Mizugaki, K. Jitsukawa and K. Kaneda, *Chem. Commun.*, 2008, **44**, 4804–4806.

13 W. Fang, J. Chen, Q. Zhang, W. Deng and Y. Wang, *Chem. Eur. J.*, 2011, **17**, 1247–1256.

14 J. Chen, W. Fang, Q. Zhang, W. Deng and Y. Wang, *Chem. Asian J.*, 2014, **9**, 2187–2196.

15 R. K. Marella, C. K. P. Neeli, S. R. R. Kamaraju and D. R. Burri, *Catal. Sci. Technol.*, 2012, **2**, 1833–1838.

16 J. Yi, J. T. Miller, D. Y. Zemlyanov, R. Zhang, P. J. Dietrich, F. H. Ribeiro, S. Suslov and M. M. Abu-Omar, *Angew. Chem. Int. Ed.*, 2014, **53**, 833–836.

17 K. Shimizu, K. Sugino, K. Sawabe and A. Satsuma, *Chem. Eur. J.*, 2009, **15**, 2341–2351.

18 K. Shimizu, K. Kon, M. Seto, K. Shimura, H. Yamazaki and J. N. Kondo, *Green Chem.*, 2013, **15**, 418–424.

19 K. Shimizu, K. Kon, K. Shimura and S. S. M. A. Hakim, *J. Catal.,* 2013, **300**, 242–250.

20 K. Kon, S. M. A. H. Siddiki and K. Shimizu, *J. Catal*, 2013, **304**, 63–71.

21 a) S. Koso, H. Watanabe, K. Okumura, Y. Nakagawa and K. Tomishige, *J. Phys. Chem, C* 2012, **116**, 3079–3090; b) Y. Amada, Y. Shinmi, S. Koso, T. Kubota, Y. Nakagawa and K. Tomishige, *Appl. Catal. B* 2011, **105**, 117 – 127; c) N. Ota, M. Tamura, Y. Nakagawa, K. Okumura and K. Tomishige; *Angew. Chem. Int. Ed*. 2015, ***54***, 1897–1900.

22 R. J. C. Brown, S. L. Segel, *Acta Cryst.*, 1980, **B36**, 2195–2198.

23 K. Shimizu, Y. Kamiya, K. Osaki, H. Yoshida and A. Satsuma, *Catal. Sci. Technol.*, 2012, **2**,

767–772.
24 K. Shimizu, T. Oda, Y. Sakamoto, Y. Kamiya, H. Yoshida and A. Satsuma, *Appl. Catal. B*, 2012, **111**–**112**, 509–514.
25 K. Kunimori, T. Uchijima, M. Yamada, H. Matsumoto, T. Hattori and Y. Murakami, *Appl. Catal.*, 1982, **4**, 67–81.
26 M. Tamura, K. Kenichi, A. Satsuma and K. Shimizu, *ACS Catal.*, 2012, **2**, 1904−1909.
27 M. Gómez-Gallego and M. A. Sierra, *Chem. Rev.*, 2011, **111**, 4857–4963.
28 T. Tanabe, Y. Nagai, T. Hirabayashi, N. Takagi, K. Dohmae, N. Takahashi, S. Matsumoto, H. Shinjoh, J. N. Kondo, J. C. Schouten and H. H. Brongersma, *Appl. Catal. A*, 2009, **370**, 108–113.
29 R. T. Sanderson, *Chemical Bond and Bond Energy*, Academic Press, New York, 1976.
30 A. L. Allred and E. G. Rochow, *J. Inorg. Nucl. Chem.*, 1958, **5**, 264–268.

Table 1. Curve-fitting analysis of Re L_3-edge EXAFS of the samples prepared by H_2-reduction of ReO_X/Al_2O_3 at different temperatures (T_{H2}).

T_{H2}/°C	Shell	N [a]	*R* /Å [b]	σ /Å [c]	R_f (%) [d]
-[e]	O	4.8	1.74	0.049	1.1
200	O	2.4	1.74	0.045	1.3
300	O	1.6	2.01	0.050	5.7
	Re	5.6	2.74	0.085	
400	O	1.5	2.10	0.020	3.2
	Re	8.1	2.74	0.075	
500 [f]	Re	8.9	2.74	0.069	3.5

a Coordination number.

bBond distance.

c Debye-Waller factor.

d Residual factor.

e ReO_X/Al_2O_3.

f The standard Re/Al_2O_3 catalyst.

Table 2. Dehydrogenation of various alcohols by Re/Al_2O_3 (reduced at 500 °C).

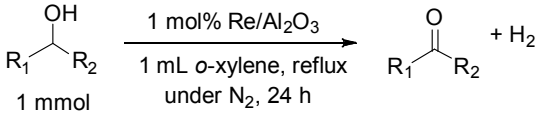

Entry	Alcohol	Conv. (%)	Yield (%)
1	Cyclooctanol	100	84
2	Cyclododecanol	93	84
3	exo-Norborneol	71	58
4	4-Octanol	96	96
5	2-Octanol	76	71
6[a]	2-Propanol	72	72
7	1-Octanol	7	1

a Reflux conditions in 1mL toluene.

Table 3. List of 5 wt% Re-loaded catalysts.

Catalyst [a]	EN [b]	T_{H2} [c] / °C	D [d] / nm
Re/MgO	2.07	400	5.4
Re/Y_2O_3	2.21	300	5.7
Re/La_2O_3	2.30	400	6.6
Re/CeO_2	2.35	600	4.1
Re/Al_2O_3	2.47	500	4.6 (5.2) [e]
Re/TiO_2	2.53	500	3.7
Re/Nb_2O_5	2.60	300	4.5
Re/SnO_2	2.76	300	6.3
Re/SiO_2	2.77	500	4.2
Re/C	-	500	3.9

a Re loading is 5 wt%.

b The averaged electronegativity of metal oxides is calculated according to the concept of Sanderson[29] on the basis of electronegativity of the element defined in ref. 30.

c Reduction temperature of the catalysts under H_2 flow.

d Average particle size (nm) of the supported Re estimated from the CO adsorption experiment.

e Average particle size (nm) of the supported Re estimated from the TEM.

Table 4. Dehydrogenation of 2-octanol by 5 wt% Re-loaded catalysts listed in Table 3.

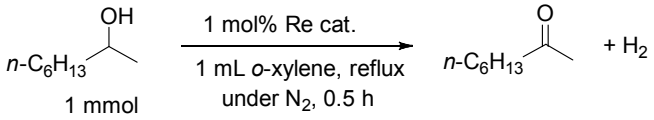

Catalyst	Conv. (%)	Yield (%)	Rate [a] /mol mol_{Re}^{-1} h^{-1}	TOF [b] / h^{-1}
Re/MgO	2	2	4	36
Re/Y_2O_3	10	5	10	94
Re/La_2O_3	5	3	6	66
Re/CeO_2	22	21	42	290
Re/Al_2O_3	21	21	42	314
Re/TiO_2	21	20	40	250
Re/Nb_2O_5	12	10	20	150
Re/SnO_2	8	4	8	85
Re/SiO_2	1	1	2	14
Re/C	3	2	4	26

a Initial rate defined as mole of 2-octanone h^{-1} per mole of Re.

b TOF defined as mole of 2-octanone h^{-1} per mole of surface Re (from CO adsorption data).

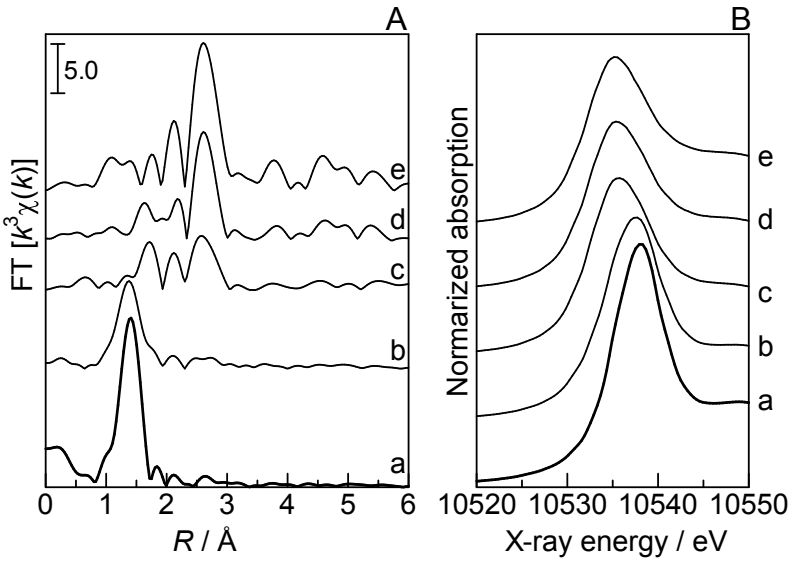

Fig. 1. Re L_3-edge (A) EXAFS Fourier transforms and (B) XANES spectra of Re-loaded Al_2O_3 samples: (a) unreduced ReO_X/Al_2O_3 and 5 wt% Re/Al_2O_3 reduced at (b) 200 °C, (c) 300 °C, (d) 400 °C, (e) 500 °C.

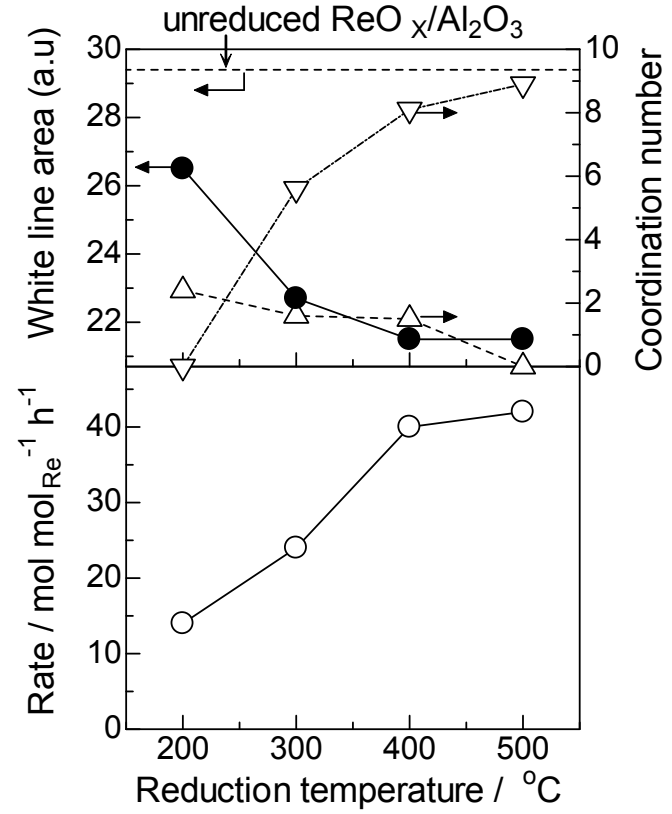

Fig. 2. Effect of H_2-reduction temperature of 5 wt% Re/Al_2O_3 on (○) the reaction rate based on the total number of Re atom for the dehydrogenation of 2-octanol, (●) area of the white line peak (XANES analysis) and coordination number of (△) Re-O and (▽) Re-Re bonds (EXAFS analysis).

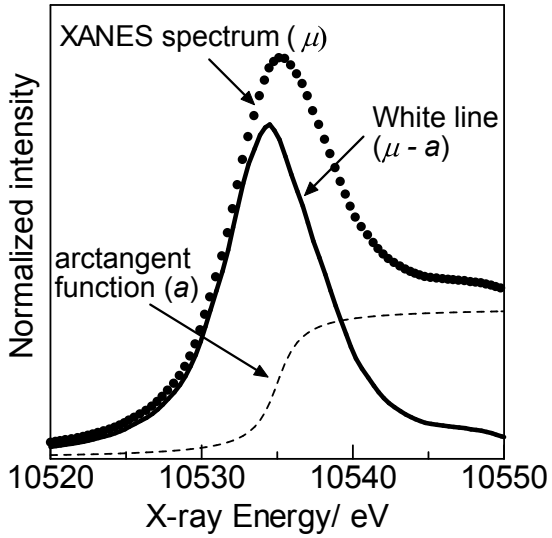

Fig. 3. An example of the Re L_3-edge XANES analysis (5 wt% Re/Al_2O_3 reduced at 500 °C). An arctangent function (dashed line) for the continuum absorption is subtracted from the raw spectrum (●) to give a function corresponding to the white line peak (solid line).

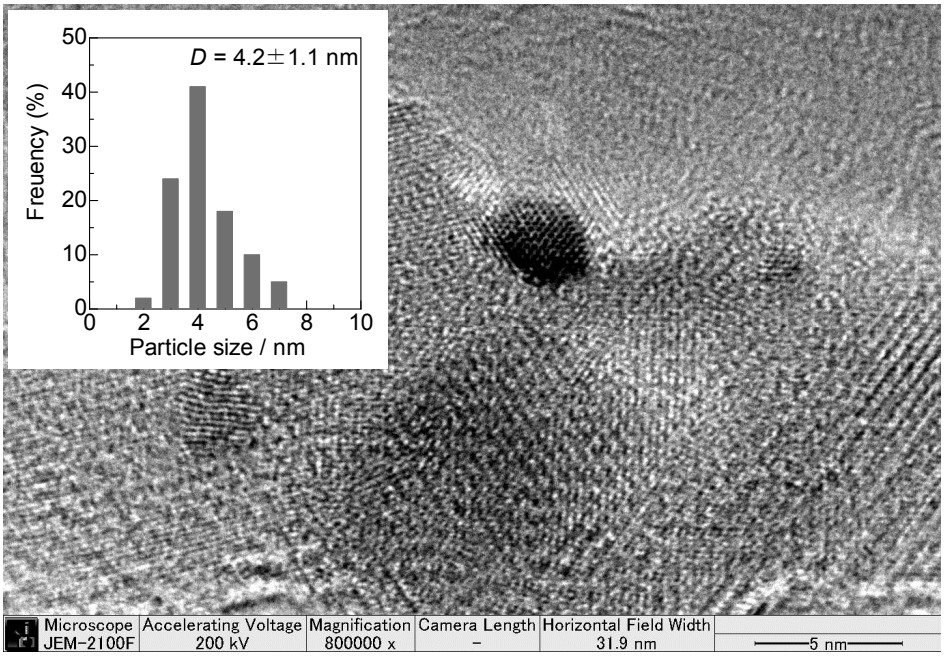

Fig. 4. A representative TEM image and Re metal particle size distribution of Re/Al_2O_3 (reduced at 500 ^oC). The mean diameter (nm) of Re particle was 4.2 ± 1.1 nm, corresponding to the volume-area mean diameter of 5.2 ± 1.1 nm.

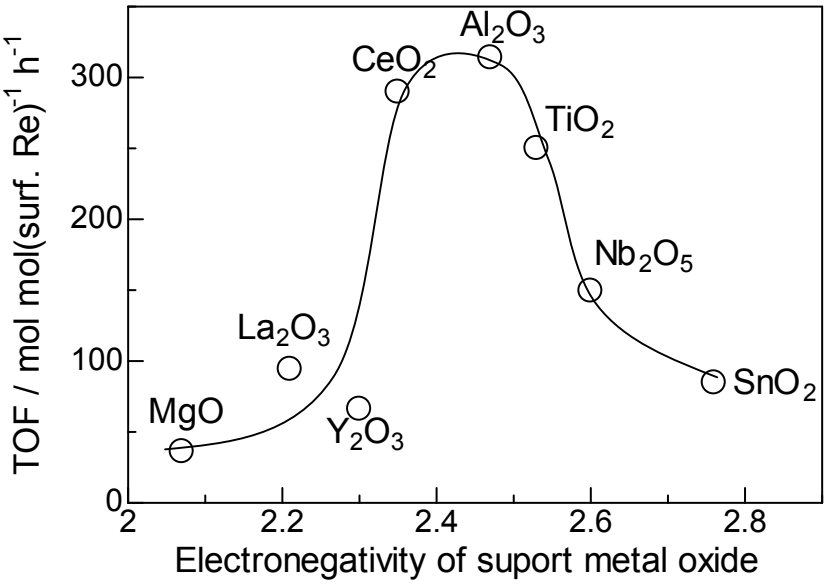

Fig. 5. Effect of the electronegativity of the metal oxide support on TOF per surface Re atom for dehydrogenation of 2-octanol by 5 wt% Re-loaded metal oxides with similar Re particle size (Table 3).

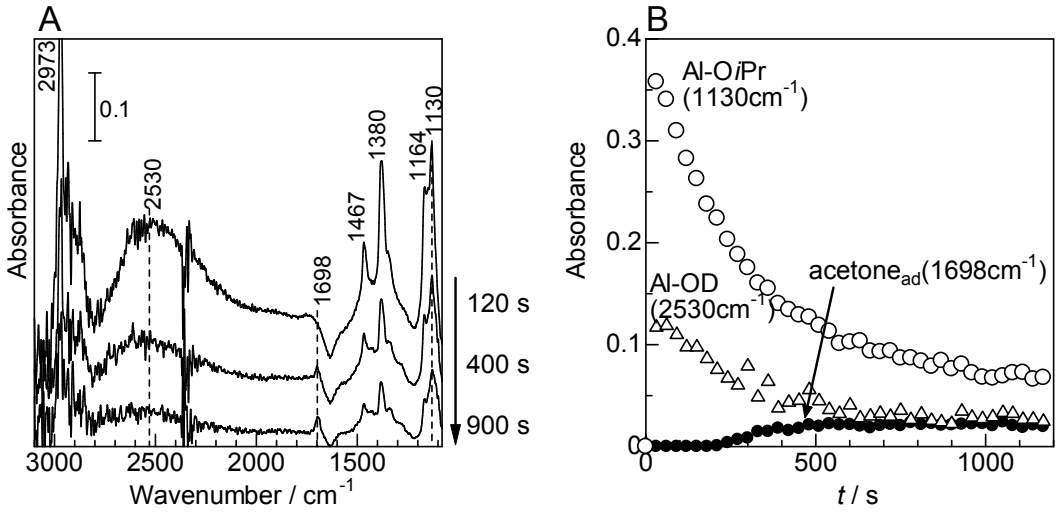

Fig. 6. (A) IR spectra of adsorbed species on Re/Al_2O_3 (reduced at 500 °C) and (B) time course of the height of the bands due to (○) 2-propoxide on the support (1130 cm^{-1}), (●) adsorbed acetone (1698 cm^{-1}), and (△) Al-OD group (2530 cm^{-1}) in a flow of He at 80 °C. At t = 0 s, 0.5 mmol g^{-1} of $(CH_3)_2CHOD$ was introduced to the catalyst.

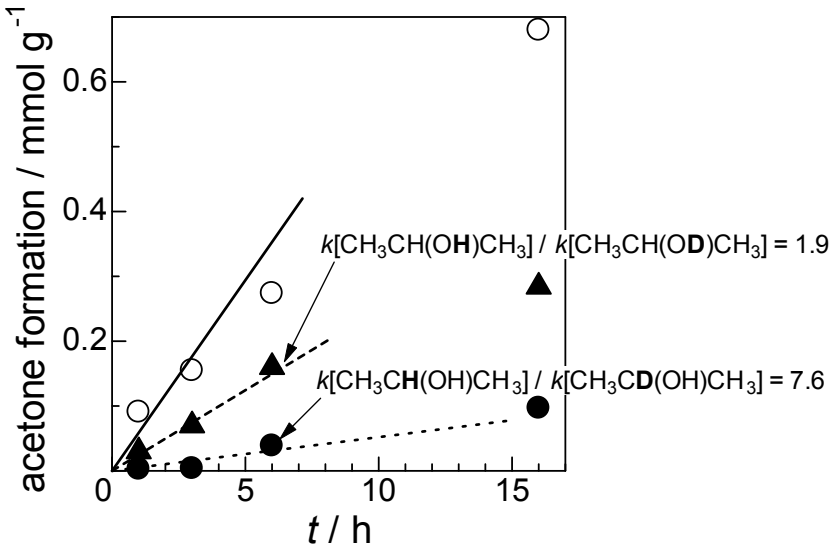

Fig. 7. Kinetic isotopic effects in the dehydrogenation of (○) 2-propanol, (▲) 2-propanol-O-d, (●) and 2-propanol-2-d1 by Re/Al_2O_3 (1 mol%): Conditions: 2-propanol (0.5 mmol), toluene (1 mL), 80 °C. Kinetic isotope effects estimated from the zero order rate constants (the slope of the lines) are shown.